Chiara Calderini, Chiara Ferrero, Pere Roca

Experimental and numerical response of dry-joint masonry arches subject to large support displacements*

1. *Introduction*

Support displacements are one of the primary sources of damage for masonry arches, which are sensitive to small changes in the boundary conditions. The potential causes of support displacements are numerous, including foundation settlements, leaning of supporting pillars, soil heterogeneity, subsidence, and landslides. Although the movements produced by these phenomena are generally small in their instantaneous values, they can result in severe damage and even collapse if they increase significantly over time (Ochsendorf, 2006). Large support displacements are thus acknowledged as a major threat to the stability of masonry arches.
Considerable research effort has been made in the last two decades to assess the stability of masonry arches under large support displacements. Both experimental testing and analytical/numerical methods were used for this purpose.
As for the experimental tests, several authors tested small- or full-scale models of masonry arches under different configurations of support displacements. As described in Ferrero, Calderini, Roca (2022a), small-scale models were more widely used with respect to full-scale ones because they are less expensive and faster to be assembled, do not require significant building skills, and allow tests to be repeated several times. Furthermore, when dealing with masonry constructions, models at reduced scale can be confidently used to simulate full-scale structures as stability

* This work is based on the following research works: Ferrero *et al.*, 2021b; Ferrero, Calderini, Roca, 2022a; Ferrero, Calderini, Roca, 2022b; Ferrero *et al*., 2021a.

Acknowledgements: The financial support of PRIN 2015 Program by the Italian Ministry of Education, University and Research (MIUR) is gratefully acknowledged for funding the research project “Protecting the Cultural Heritage from water-soil interaction related threats” (Prot. No. 2015EAM9S5), which is the main framework of the study presented in this article.

is a matter of geometry rather than material failure (Heyman, 1995). Since the strength of the composing material is irrelevant, the small-scale models were built using a number of materials, including concrete, stainless steel, bricks, and wood, among the others. The voussoirs were assembled either with mortar or dry joints. The large majority of the experimental tests were carried out on arches subjected to horizontal and vertical support displacements, while little attention was devoted to inclined support displacements (Ferrero, Calderini, Roca, 2022a).

As for the analytical and numerical methods, a growing number of methods and procedures has been developed to investigate the response of masonry arches to large support displacements. The large majority of these methods modelled arches as rigid-no tension structures by adopting the three simplified assumptions introduced by Heyman (1966, 1995) to describe the behaviour of masonry materials: (I) infinite compressive strength, (II) no tensile strength, and (III) no sliding failure. Starting from these hypotheses, which provide the theoretical basis for the Limit Analysis theory, some authors proposed analytical and computational methods based on a standard application of the static and kinematic theorems of Limit Analysis (e.g., Block, Ciblac, Ochsendorf, 2006; Coccia, Di Carlo, Rinaldi, 2015; Di Carlo, Coccia, 2020; McInerney, DeJong, 2015; Ochsendorf, 2002, 2006; Romano, 2005; Romano, Ochsendorf, 2010; Zampieri *et al*., 2018a, 2018b; Zampieri, Simoncello, Pellegrino, 2018). Other authors developed procedures that, although adopting Heyman's assumptions on the behaviour of masonry structures, went beyond the standard application of the theorems of Limit Analysis (e.g., Ferrero *et al.*, 2021a; Galassi *et al.*, 2018; Galassi *et al.,* 2019; Galassi, Misseri, Rovero, 2021; Iannuzzo *et al.*, 2021; Portioli, Cascini, 2017). Finally, some authors used discrete element (DE) and finite element (FE) methods under Heyman's assumptions (e.g., Ayensa *et al.*, 2015; Ferrero *et al.*, 2021a, 2021b; Iannuzzo *et al.*, 2021; McInerney, DeJong, 2015; Zampieri *et al.*, 2018a). Similarly to what observed in the case of the experimental tests, also in the case of the analytical and numerical methods the largest attention was devoted to vertical and horizontal supports displacements, whereas inclined support displacements were little investigated (Ferrero *et al*., 2021a).

The large majority of the above-mentioned analytical and numerical methods were validated against the results from experimental tests on small- or full-scale models of arches with mortar or dry joints. As described in Ferrero *et al.* 2022b, when treating arches as rigid-no tension structures, the analytical and numerical procedures generally well captured the experi-

mental response in terms of opening of the initial hinges, hinge location, and collapse mechanisms, but they overestimated the experimental ultimate displacement capacity. This discrepancy was attributed to the imperfections of the physical models, which negatively affect stability and cause collapse to occur for a smaller support displacement than that predicted by perfect analytical/numerical models (Ochsendorf 2002, 2006; Galassi *et al.*, 2018).

In view of the foregoing, this work aims at (I) developing a deep understanding of the response of masonry arches to inclined support displacements and (II) proposing a numerical approach able to accurately simulate the behaviour exhibited by these structural elements when subjected to large support displacements. To accomplish these goals, a 1:10 small-scale model of a segmental dry-joint masonry arch was first tested to collapse under vertical, horizontal, and inclined support displacements. The experimental tests were then numerically simulated adopting a FE micro-modelling approach, in which the arch was schematized as an assemblage of voussoirs, very stiff and infinitely resistant in compression, interacting at no-tension friction interfaces. The arch response to large support displacements was assessed by means of nonlinear static analyses, in which support displacements were increased monotonically up to collapse. The proposed numerical approach was validated through comparison with the experimental results.

The present work is organized as follows. In Section 2, the experimental tests and results are presented. In Section 3, the adopted FE micro-modelling approach is described. In Section 4, the numerical predictions are compared with the experimental results. In Section 5, some conclusions are drawn.

2. *Experimental testing*

2.1. *Description of the physical model*

The experimental tests, presented in Ferrero, Calderini, Roca (2022a), Ferrero *et al.* (2021a) and Ferrero (2021), were performed on a 1:10 small-scale model of a segmental dry-joint masonry arch supported by two piers **[fig. 1a]**. The arch has an angle of embrace of 125°, a span length (L) of 533 mm, a radial thickness of 24 mm and a rise of 162 mm. It consists of 55 voussoirs with dimensions 24 x 12 x 120 mm^3 and slightly trapezoidal shape to compensate for the lack of mortar joints. As described more in

detail in Ferrero *et al.* (2021a, 2021b), the geometry of the arch is representative of the cross-section of a two-course brick barrel vault with a radial thickness of 0.24 m and an internal radius of 3 m.
The blocks of the mockup (both voussoirs and piers) were made of a bicomponent composite material (Plastoform PL, Prochima, 2009), which was obtained by mixing a mineral powder with an acrylic polymer in aqueous solution. The blocks were produced by pouring the mixture into special silicone moulds **[fig. 1c]** created from aluminium matrices shaped as the blocks **[fig. 1d]**. In the case of the voussoirs, the mixture was fluidified by adding a plasticizer (1% of the total weight) to facilitate the pouring.
The mockup was built as a dry-joint assemblage of bicomponent composite blocks because this manufacturing technique allowed the small-scale model to be coherent with Heyman's assumptions on the behaviour of masonry structures. The blocks had high compressive stress and stiffness with respect to the applied loads and, thus, could be considered rigid and infinitely resistant in compression. Furthermore, the dry joints had zero tensile strength and a high friction angle which caused sliding not to occur.
The friction angle (μ), compressive strength (σ_c) and Young's modulus (E) of the blocks were respectively equal to 41.2° (corresponding to a friction coefficient of 0.7), 9.1 MPa, and 941 MPa, as measured experimentally (Ferrero *et al.*, 2022a). The density (ρ) of the bicomponent composite material was 1640 kg/m^3. The total weight of the mockup (including arch and supporting piers) was about 13.9 kg.
The arch was tested to collapse by moving the right support at a very low speed (maximum 0.04 mm/s) in vertical, horizontal, or inclined direction. Thirteen displacement directions were investigated by varying the angle α, which identifies the direction of the imposed displacement δ, between 0° and 90° **[fig. 1a]**. Since the angle α was measured from the vertical, α = 0° and α = 90° correspond to purely vertical and horizonal support displacements, respectively. The vertical and horizontal components of the imposed displacement δ, respectively named δ_z and δ_x **[fig. 1a]**, are expressed in a dimensionless form as δ_z/L and δ_x/L, where L is the arch span length.

2.2. *Results*

The arch response to large support displacements was assessed in terms of collapse mechanisms, evolution of the hinge configuration, and ultimate displacement capacity. The main conclusions drawn from the exper-

imental tests are reported in this section, while the reader is referred to Ferrero, Calderini, Roca (2022a) and Ferrero (2021a) for an in-depth analysis of the experimental results.

No matter the direction of the imposed support displacements, the arch initially opened three hinges, hereafter labelled A, B and C (beginning from the left support). For α between 0° and 75°, collapse was reached when a fourth hinge (hereafter indicated as D) opened at the left support. In the case of α = 90° only, due to the symmetry in geometry and displacement loading, a fifth hinge (E) also appeared at collapse at the right support.

Fig. 2 shows the collapse mechanisms obtained for four representative values of α (0°, 20°, 60°, 90°). Since hinges A, B and C may change position with the increase of support displacements, both their initial (A_0, B_0, C_0) and final (A_u, B_u, C_u) locations are indicated. The hinge position was found to depend on the direction of the support displacements. Based on the initial and final positions of hinges A, B and C, three modes of evolution of the hinge configuration with increasing support displacements were identified when varying α. The three modes can be described as follows:

- *Mode I* (for α between 0° and 15°, **fig. 2a**). The three initial hinges A, B and C follow the sequence I-E-E (from the left fixed support, where I = intrados and E = extrados) for every value of imposed displacement and do not generally move as support displacements increase. Collapse occurs by an asymmetrical four-hinge mechanism when hinge D opens at the left support at the extrados (sequence E-I-E-E).
- *Mode II* (for α equal to 20°, **fig. 2b**). The three initial hinges A, B and C are initially located according to the sequence I-E-E. As support displacements increase, hinge C closes at the extrados (right support) and opens at the intrados (right haunch). As a result, failure is governed by an asymmetrical four-hinge collapse mechanism with hinges located in the sequence E-I-E-I.
- *Mode III* (for α between 25° and 90°, **fig. 2c-d**). Hinges A, B and C alternate between the intrados and the extrados (sequence I-E-I) for every value of imposed displacement. The intrados hinges A and C generally move upwards towards the crown as the right support moves. For values of α up to 75° **[fig. 2c]**, collapse occurs by an asymmetrical four-hinge mechanism with hinges located according to the sequence E-I-E-I. For α equal to 90° **[fig. 2d]**, the arch collapses by an almost symmetrical five-hinge mechanism with two hinges (D and E) occurring at the springings (sequence E-I-E-I-E).

It is interesting to note that, for α between 20° and 30°, hinge C appeared in the form of minor openings distributed over consecutive joints. These minor and distributed openings (indicated in **fig. 2b** with dotted circles) were found to have the same effect as a hinge in the activation of the collapse mechanism (Ferrero et al, 2022a). As shown in **fig. 2b** for α = 20°, when hinge C occurred in the form of minor openings distributed, the thrust line at collapse (drawn on the arch deformed configuration by using graphic statics, see Heyman, 1992 and Huerta, 2011) did not touch the arch intrados at the right haunch, as expected in the case of a fully developed hinge, but it was almost tangent to it in correspondence to several consecutive joints. This behaviour differs from that expected for a rigid-no tension arch, which collapses when (at least) four fully developed hinges appear and the thrust line is tangent to the arch profile in at least four points (Heyman, 1995).
Fig. 3 shows the limit displacement domain of the tested arch, which was obtained by plotting the normalized vertical collapse displacement $\delta_{z,u}/L$ versus the normalized horizontal collapse displacement $\delta_{x,u}/L$ for every value of α. This domain, introduced for the first time by the authors in Ferrero *at al*. (2021a), indicates the combinations of vertical and horizontal displacements that the arch can withstand safely (points below the boundary of the domain) as well as those that cause collapse (boundary of the domain and points above it). Different trends in the variation of the collapse displacements with α can also be identified, which correspond to the different *modes* of evolution of the hinge configuration (for further details the reader is referred to Ferrero, Calderini, Roca, 2022a). Looking at **fig. 3**, it can also be seen that the arch had a significantly larger capacity to withstand vertical support displacements compared to horizontal support displacements. The vertical and horizontal collapse displacements obtained for α equal to 0° and 90° were equal to about 16.5% and 3.7% of the arch span length, respectively.

3. *Numerical modelling*

The numerical simulations were performed using the commercial FEM software DIANA FEA (TNO DIANA BV, 2014). A two-dimensional plane stress model of the tested arch, not including the supporting piers, was created in Midas FX+ Customized Pre/Post-processor for DIANA software (FX+ for DIANA, 2011). Following a micro-modelling approach, the arch was schematized as an assemblage of units, representing in size and shape

the real voussoirs, and zero-thickness interfaces, representing the dry joints. Further interface elements were placed at the arch springings to allow hinges to open at the supports. The edges of these interfaces were pinned to provide boundary conditions.

The mesh of the FE model was created using four-node quadrilateral isoparametric plane stress elements (Q8MEM) for the voussoirs and 2D four-node line interface elements (L8IF) for the interfaces. Following Ferrero *et al.*, (2021a, 2021b), a mesh size of 2 mm, corresponding to having twelve FEs along the arch radial thickness, was adopted.

The voussoirs were modelled as linear elastic elements with infinite compressive strength. The Young's modulus E = 941 MPa and the density ρ = 1640 kg/m^3 were taken equal to the values measured experimentally (see **Section 2**), while a Poisson's ratio of 0.2 was assumed.

All the nonlinearities were concentrated in the interfaces, which were modelled adopting a Coulomb friction model with cohesion and dilatancy angle set to zero. The friction coefficient μ was taken equal to 0.7, as measured experimentally. The friction model was extended with a gap criterion with zero tensile strength to allow hinges to open when tensile stresses arise. For further details about the Coulomb friction model and the gap criterion, the reader is referred to TNO DIANA BV (2014).

Special attention was devoted to the choice of the stiffness properties to be adopted for the interface elements, since they play a crucial role in the FE micro-modelling of dry-joint masonry arches (Ferrero *et al.*, 2021a, 2021b; Gaetani *et al.*, 2017; Lourenço *et al.*, 2010). The use of a Coulomb friction model requires to define two values of interface stiffness: the interface normal stiffness k_n and the interface tangential stiffness k_s. Since these properties were not measured experimentally, their effect on the numerical results was evaluated through a sensitivity analysis. Following the approach adopted in Ferrero *et al.* (2021a, 2021b), the interface normal stiffness k_n was varied within a range defined based on literature, whereas the interface tangential stiffness k_s was set equal to $0.5k_n$ for every value of k_n adopted. The effect of the interface normal stiffness on the arch response was first assessed for α = 0° (purely vertical displacements) by considering several values of k_n (**Section 4.1**). Subsequently, based on the results obtained, two reference values of k_n were chosen and adopted to analyse the arch behaviour when varying the direction of support displacements (**Section 4.2**).

Nonlinear static analyses were performed to simulate the experimental tests. First, self-weight was applied and then support displacements were

increased monotonically up to collapse. A regular Newton-Raphson iteration method was adopted in combination with a line search algorithm (TNO DIANA BV, 2014). To verify convergence, an energy-based convergence criterion with a tolerance value of 0.001 was assumed. Geometric nonlinearities were considered by adopting the Total Lagrange formulation available in DIANA (TNO DIANA BV, 2014).

4. *Comparison between experimental and numerical results*

4.1. *Sensitivity analysis for α = 0°*

In this section, the numerical and experimental results are compared for α = 0° in terms of collapse mechanism, hinge position at collapse and ultimate displacement capacity. The sensitivity of the FE predictions to the interface normal stiffness k_n is also evaluated by varying k_n between 0.1 and 100 N/mm^3, as proposed in Ferrero *et al.* (2021a, 2021b).
Fig. 4a-b-c-d reports the collapse mechanisms obtained for four representative values of k_n. Regardless of k_n, collapse occurred by an asymmetrical four-hinge mechanism with hinges located according to the sequence E-I-E-E. As observed in the experimental tests, hinges A, B and C were the first hinges to appear, whereas hinge D opened at collapse. As already commented in Ferrero *et al.* (2021a, 2021b), for small values of k_n, the hinges moved inward with respect to the intrados or extrados line of the arch due to the large interpenetration of adjacent blocks and, thus, generally appeared in the form of minor openings distributed over consecutive interfaces. In contrast, as k_n increased, they concentrated in fewer interfaces and moved towards the arch profile because of the smaller block interpenetration. For values of k_n equal or larger than 10 N/mm^3 **[fig. 4c-d]**, hinges A, B, C and D opened each in one interface, in full accordance with the experimental tests, and appeared at the edge line of the arch (compressive stresses are concentrated in only one FE of each interface).
Fig. 4e and **fig. 4f** respectively show the values of the collapse displacement and the position at collapse of hinges A, B and C as a function of k_n. The collapse displacement increased with increasing k_n until reaching a maximum constant value that was not affected by any further stiffness increase **[fig. 4e]**. The hinge position at collapse **[fig. 4f]** was the same no matter k_n for hinge C, whereas it changed with k_n for hinges A and B (note that the joints where hinges appear are numbered from left to right, being joint no.1 the one at the left support). As k_n increased, hinge A and C

opened closer to the left and right support, respectively. However, in the range k_n = 48÷100 N/mm^3, hinges A and B were located at the same position regardless of k_n.
As can be seen from **fig. 4e** and **fig. 4f**, neither the ultimate displacement capacity nor the hinge location at collapse varied with the interface stiffness in the range k_n = 48÷100 N/mm^3. Consequently, for any k_n equal or larger than 48 N/mm^3, the interfaces can be considered as (almost) rigid and the arch can be treated as a rigid-no tension structure, as usually done in the literature when dealing with arches on moving supports (see **Section 1**). In Ferrero *et al.* (2021a), by comparing the FE results with the numerical predictions from a perfectly rigid block model (Portioli, Cascini, 2017), the authors actually proved that the value k_n = 48 N/mm^3 was representative of rigid interfaces.
Looking at **fig. 4e-f**, it can be seen that, if k_n is taken equal to 48 N/mm^3, the FE model significantly overestimates the experimental displacement capacity and does not accurately predict the experimental hinge position at collapse, even though it correctly simulates the experimental collapse mechanism. This outcome is in full accordance with the results from literature (see **Section 1**). In contrast, if k_n is reduced up to about 3 N/mm^3, the FE model is able to accurately predict the experimental collapse displacement and hinge position at collapse. Such a value of k_n is significantly smaller than the one used to simulate rigid (perfect) interfaces and, thus, represents rather deformable interfaces. In **Section 4.2**, k_n will be taken equal to 3 N/mm^3 and 48 N/mm^3 to perform further numerical analyses when varying α between 0° and 90°.

4.2. *Response for α = 0°÷90°: rigid vs deformable interface models*

In this section, the numerical predictions for both k_n = 3 N/mm^3 (deformable interfaces) and k_n = 48 N/mm^3 (rigid interfaces) are compared with the experimental results for all the directions of support displacements. The comparison is carried out in terms of limit displacement domain, collapse mechanisms and *modes* of evolution of the hinge configuration.
Fig. 5 shows the limit displacement domain of the arch obtained from both the experimental tests and numerical simulations. It is easy to see that the numerical model significantly overestimated the displacement capacity of the physical model for k_n = 48 N/mm^3, while it accurately predicted it for k_n = 3 N/mm^3. In the first case, the relative error between numerical and experimental collapse displacements ranged between about 22% and 53%,

while in the second case it ranged between about -5% and 5% for every α, except for 10° and 90°, for which it was equal to -6.1% and 8.5%, respectively. Despite the differences in terms of ultimate displacement capacity obtained for k_n = 48 N/mm^3, for both values of k_n the numerical model was able to predict the overall qualitative trend exhibited by the experimental limit domain (i.e., how the vertical and horizontal collapse displacements varied with α).

Fig. 6 depicts the collapse mechanisms obtained for k_n = 3 N/mm^3 (left) and k_n = 48 N/mm^3 (right) for some representative values of α (0°, 20°, 25° and 90°). The initial and final locations of three initial hinges A, B and C is also reported. For both values of k_n, the FE model was able to capture the same collapse mechanisms obtained in the experiments (see **Section 2.2**). For k_n = 3 N/mm^3 **[fig. 6 on the left]**, the FE simulations also predicted the same *modes* of evolution of the hinge configuration identified in the tests when varying α. For k_n = 48 N/mm^3, the numerical results were in full accordance with the experimental ones for every α except 25°. In this latter case, although the numerical collapse mechanism was the same as the experimental one, *mode II*, instead of *mode III,* was predicted to occur **[fig. 6c on the right]**.

Despite the good agreement between experimental and numerical results obtained in terms of collapse mechanisms and *modes* of evolution of the hinge configuration for both k_n = 3 N/mm^3 and k_n = 48 N/mm^3, the numerical model was able to accurately predict the experimental hinge location only when adopting k_n = 3 N/mm^3. This can be easily seen from Table 1, which compares the predicted and experimental positions at collapse of hinges A, B and C. For k_n = 3 N/mm^3, the numerical hinge position was generally the same as the experimental one (or differed by a maximum of one voussoir). In contrast, when adopting k_n = 48 N/mm^3, the numerical and experimental locations did not generally match. For every α, hinge A was located closer to the left support and hinge B closer to the right support in the numerical model with respect to the physical one. In the case of hinge C, the experimental and numerical positions at collapse were in full accordance only for α between 0° and 15. In contrast, for α between 20° and 90°, hinge C was located closer to the right support in the numerical model compared to the physical one.

From **Table 1**, it can also be seen that the FE model was able to catch the opening of hinge C in the form of minor and distributed openings for α between 20° and 30°, as observed in the experiments, only when adopting k_n = 3 N/mm^3. In contrast, when using k_n = 48 N/mm^3, hinge C was predicted to occur in the form of a fully developed hinge.

Table 1. Position at collapse of hinges A, B and C obtained from experimental tests and FE analyses for k_n = 3 N/mm^3 and k_n = 48 N/mm^3 (I = intrados, E = extrados, m.d.o = minor distributed openings) (Ferrero, Calderini, Roca, 2022b).

α [°]	Joint no.								
	Hinge A			Hinge B			Hinge C		
	Exp	FEM (k_n = 3 N/mm^3)	FEM (k_n = 48 N/mm^3)	Exp	FEM (k_n = 3 N/mm^3)	FEM (k_n = 48 N/mm^3)	Exp	FEM (k_n = 3 N/mm^3)	FEM (k_n = 48 N/mm^3)
0	9-I	9-I	8-I	28-I	29-I	32-I	56-E	56-E	56-E
5	9-I	9-I	8-I	31-I	31-I	32-I	56-E	56-E	56-E
10	9-I	9-I	8-I	31-I	31-I	32-I	56-E	56-E	56-E
15	10-I	10-I	8-I	31-I	31-I	32-I	56-E	56-E	56-E
20	9-I	9-I	8-I	30-I	31-I	32-I	m.d.o.-I	m.d.o.-I	48-I
25	9-I	9-I	7-I	28-I	29-I	30-I	m.d.o.-I	m.d.o.-I	48-I
30	9-I	9-10-I	7-I	28-I	29-I	29-I	m.d.o.-I	m.d.o.-I	47-I
35	10-I	9-10-I	7-I	28-I	28-I	29-I	45-I	44-45-46-I	47-I
40	10-I	10-I	8-I	28-I	28-I	29-I	44-45-46-I	44-45-46-I	47-I
45	11-I	10-I	8-I	28-I	28-I	29-I	44-45-46-I	44-45-46-I	48-I
60	11-I	10-11-I	9-I	28-I	28-I	28-I	44-I	45-I	47-I
75	11-I	11-I	9-I	28-I	28-I	29-I	45-I	45-46-I	48-I
90	12-I	11-I	9-I	28-I	27-28-I	28-29-I	45-I	46-I	48-I

The results presented in this section show that, for all the directions of support displacements investigated, adopting k_n = 3 N/mm^3 provides a much better matching between numerical and experimental outcomes with respect to k_n = 48 N/mm^3. Since assuming k_n = 48 N/mm^3 means modelling rigid interfaces, it can be concluded that the joints of the physical model are not rigid but are characterized by a certain deformability. As described in Ferrero, Calderini, Roca (2022b), this deformability can be attributed to imperfections such as the roughness and not perfect coplanarity of the contact surfaces between adjacent voussoirs, which may result from the manufacturing process of the blocks.

5. *Conclusions*

This paper investigates the response of masonry arches to large support displacements through experimental tests and numerical simulations. The experimental tests were performed on a 1:10 small-scale model of a segmental arch, which was built as a dry-joint assemblage of bicomponent composite voussoirs and was tested to collapse under vertical, horizontal, and inclined support displacements. The numerical analyses were carried

out by adopting a FE micro-modelling approach, in which the arch was schematized as an assemblage of voussoirs, very stiff and infinitely resistant in compression, connected by no-tension interfaces.
By analysing several combinations of vertical and horizontal support displacements, this paper provided a deep understanding of the behaviour exhibited by masonry arches when subjected to inclined support displacements. The direction of the support displacements was found to significantly affect the arch response in terms of collapse mechanism, evolution of the hinge configuration, and ultimate displacement capacity.
For all the directions of support displacements investigated, the comparison between experimental and numerical results was carried out using two different value of interface normal stiffness, which represented either rigid or deformable interfaces. In full accordance with the results obtained in the literature, the FE model with rigid interfaces, although accurately predicting the experimental collapse mechanisms, was found to significantly overestimate the experimental ultimate displacement capacity. This paper demonstrated that using deformable interfaces in the FE model could provide a very good matching between numerical and experimental results also in terms of ultimate displacement capacity. This outcome proved that the joints of the physical model were not fully rigid but characterized by a certain deformability, which was attributed to the presence of imperfections in the contact surfaces between adjacent voussoirs. Calibrating the interface stiffness based on the experimental results proved to be an effective strategy to accurately simulate the arch response to large support displacements and take into account the imperfections of the physical models.
Future research will be devoted to investigating the effect of the imperfections and deformability of the joints on the response of masonry arches to large support displacements. The study will be addressed to dry-joint masonry arches with different geometries as well as to masonry arches assembled with mortar joints.

References

Ayensa *et al*., 2015: Ayensa A., Beltran B., Ibarz E., Gracia L., "Application of a new methodology based on Eurocodes and finite element simulation to the assessment of a romanesque church", in *Construction and Building Materials*, 101 (2015), n. 1, pp. 287-297; DOI: https://doi.org/10.1016/j.conbuildmat.2015.10.115.

Block, Ciblac, Ochsendorf, 2006: Block P., Ciblac T., Ochsendorf J.A., 2006. "Real-time limit analysis of vaulted masonry buildings", in *Computers & Structures*, 84 (2006), nn. 29-30, pp. 1841-1852; DOI: https://doi.org/10.1016/j.compstruc.2006.08.002.

Coccia, Di Carlo, Rinaldi, 2015: Coccia S., Di Carlo F., Rinaldi Z., "Collapse displacements for a mechanism of spreading-induced supports in a masonry arch", in *International Journal of Advanced Structural Engineering*, 7 (2015), n. 3, pp. 307-320; DOI: https://doi.org/10.1007/s40091-015-0101-x.

Di Carlo, Coccia, 2020: Di Carlo F., Coccia S., "Collapse state of elliptical masonry arches after finite displacements of the supports", in *Engineering Failure Analysis*, 114 (2020); DOI: 10.1016/j.engfailanal.2020.104593.

Ferrero, 2021: Ferrero C., *Structural behaviour of masonry arches on moving supports: from on-site observation to experimental and numerical analysis,* PhD dissertation, University of Genoa-Technical University of Catalonia, 2021.

Ferrero *et al*., 2021a: Ferrero C., Calderini C., Portioli F.P., Roca P., "Large displacement analysis of dry-joint masonry arches subject to inclined support movements", in *Engineering Structures*, 238 (2021); DOI: https://doi.org/10.1016/j.engstruct.2021.112244.

Ferrero *et al*., 2021b: Ferrero C., Rossi M., Roca P., Calderini C., "Experimental and numerical analysis of a scaled dry-joint arch on moving supports", in *International Journal of Masonry Research and Innovation*, 1 (2021), n. 1, pp. 405-421; DOI: https://doi.org/10.1504/IJMRI.2021.10035577.

Ferrero, Calderini, Roca, 2022a: Ferrero C., Calderini C., Roca P., "Experimental response of a scaled dry-joint masonry arch subject to inclined support displacements", in *Engineering Structures*, 253 (2022); DOI: https://doi.org/10.1016/j.engstruct.2021.113804.

Ferrero, Calderini, Roca, 2022b: Ferrero C., Calderini C., Roca P., "Prediction of the response of masonry arches to large support displacements: comparison of no-tension rigid and flexible interface models", in *Engineering Structures*, 2022 (under review).

FX+ for DIANA. *Midas FX+ for DIANA, Customized Pre/Post-processor for DIANA*, 2013.

Gaetani *et al*., 2017: Gaetani A., Lourenço P.B., Monti G., Moroni M., "Shaking table tests and numerical analyses on a scaled dry-joint arch undergoing windowed sine pulses", in *Bulletin of Earthquake Engineering*, 15 (2017), pp. 4939-4961.

Galassi *et al*., 2018: Galassi S., Misseri G., Rovero L., Tempesta G., "Failure modes prediction of masonry voussoir arches on moving supports", in *Engineering Structures*, 173 (2018), pp. 706-717; DOI: https://doi.org/10.1016/j.engstruct.2018.07.015.

Galassi *et al*., 2019: Galassi S., Misseri G., Rovero L., Tempesta G., "Analysis of Masonry Pointed Arches on Moving Supports: A Numeric Predictive Model and Experimental Evaluations", in *Proceedings of XXIV AIMETA Conference 2019*, 15-19 September 2019, Rome, Italy, pp. 1-21.

Galassi, Misseri, Rovero, 2021: Galassi S., Misseri G., Rovero L., "Capacity assessment of masonry arches on moving supports in large displacements: Numerical model and experimental validation", in *Engineering Failure Analysis,* 129 (2021); DOI: https://doi.org/10.1016/j.engfailanal.2021.105700.

Heyman, 1966: Heyman J., "The stone skeleton", in *International Journal of Solids Structures*, 2 (1966), n. 2, pp. 249-279.

Heyman, 1982: Heyman J., *The masonry arch*, Chichester, Ellis Horwood Ltd, 1982.

Heyman, 1995: Heyman J., *The stone skeleton*, Cambridge, Cambridge University Press, 1995.

Huerta, 2011: Huerta S., "The analysis of masonry architecture: A historical approach", in *Architectural Science Review*, 51 (2011), n. 4, pp. 297-328.

Iannuzzo *et al*., 2021: Iannuzzo A., Dell'Endice A., Van Mele T., Block P., "Numerical limit analysis-based modelling of masonry structures subjected to large displacements", in *Computers & Structures*, 242 (2021); DOI: https://doi.org/10.1016/j.compstruc.2020.106372.

Lourenço *et al*., 2010: Lourenço P.B., Hunegn T., Medeiros P., Peixinho N., "Testing and analysis of masonry arches subjected to impact loads", in *Proceedings of the 6th International Conference on Arch Bridges (ARCH'10)*, 11-13 October 2010, Fuzhou, China, pp. 603-610.

McInerney, DeJong, 2015: McInerney J., DeJong M.J., "Discrete Element Modelling of Groin Vault Displacement Capacity", in *International Journal of Architectural Heritage*, 9 (2015), n. 8, pp. 1037-1049; DOI: https://doi.org/10.1080/15583058.2014.923953.

Ochsendorf, 2002: Ochsendorf J.A., *Collapse of masonry structure,* PhD dissertation, University of Cambridge, 2002.

Ochsendorf, 2006: Ochsendorf J.A., "The masonry arch on spreading supports", in *Structural Engineer*, 84 (2006), n. 2, pp. 29-35.

Plastoform PL, Prochima, 2009: Prochima. *Plastoforma PL; Technical data sheet,* 2019. Accessed July 14, 2019; <https://www.prochima.it/files/PLASTOFORMA-PL_versione-6.pdf>.

Portioli, Cascini, 2017: Portioli F.P., Cascini L., "Large displacement analysis of dry-jointed masonry structures subjected to settlements using rigid block modelling", in *Engineering Structures*, 148 (2017), pp. 485-496; DOI: https://doi.org/10.1016/j.engstruct.2017.06.073.

Romano, Modelling, 2005: *Modelling, analysis and testing of masonry structures*. PhD dissertation, University of Naples Federico II, 2005.

Romano, Ochsendorf, 2010: Romano A., Ochsendorf J.A., "The mechanics of gothic masonry arches", *in International Journal of Architectural Heritage*, 4 (2010), n. 1, pp. 59-82; DOI: https://doi.org/10.1080/15583050902914660.

TNO DIANA BV: *DIANA Finite Element Analysis User's Manual Release 9.6*, Delft, The Netherlands, 2014.

Zampieri *et al*., 2018a: Zampieri P., Faleschini F., Zanini M.A., Simoncello N., "Collapse mechanisms of masonry arches with settled springing", in *Engineering Structures*, 156 (2018), pp. 363-374; DOI: https://doi.org/10.1016/j.engstruct.2017.11.048.

Zampieri *et al*., 2018b: Zampieri P., Cavalagli N., Gusella V., Pellegrino C., "Collapse displacements of masonry arch with geometrical uncertainties on spreading supports", in *Computers & Structures*, 208 (2018), pp. 118-129; DOI: https://doi.org/10.1016/j.compstruc.2018.07.001.

Zampieri, Simoncello, Pellegrino, 2018: Zampieri P., Simoncello N., Pellegrino C., "Structural behaviour of masonry arch with no-horizontal springing settlement", in *Frattura ed Integrità Strutturale*, 12 (2018), n. 3, pp. 182-190; DOI: https://doi.org/10.3221/IGF-ESIS.43.14.

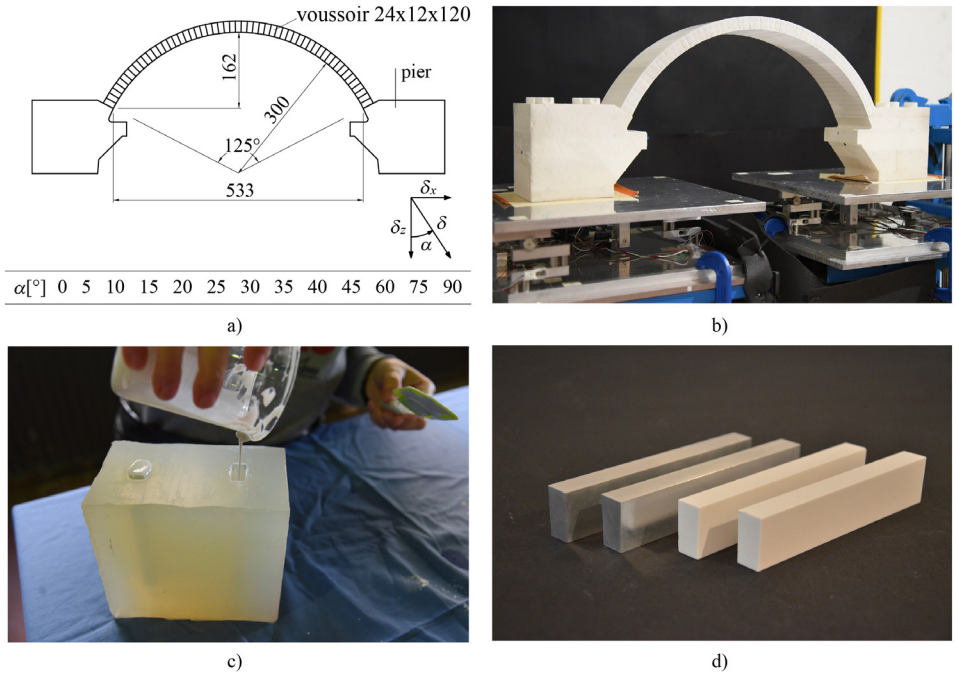

Fig. 1. a) Geometry of the mockup (dimensions in mm) and investigated displacement direction, b) view of the physical model, c) silicone mould used for the production of the arch voussoirs, d) alluminium matrices and bicomponent composite blocks (Ferrero, Calderini and Roca, 2022a-b).

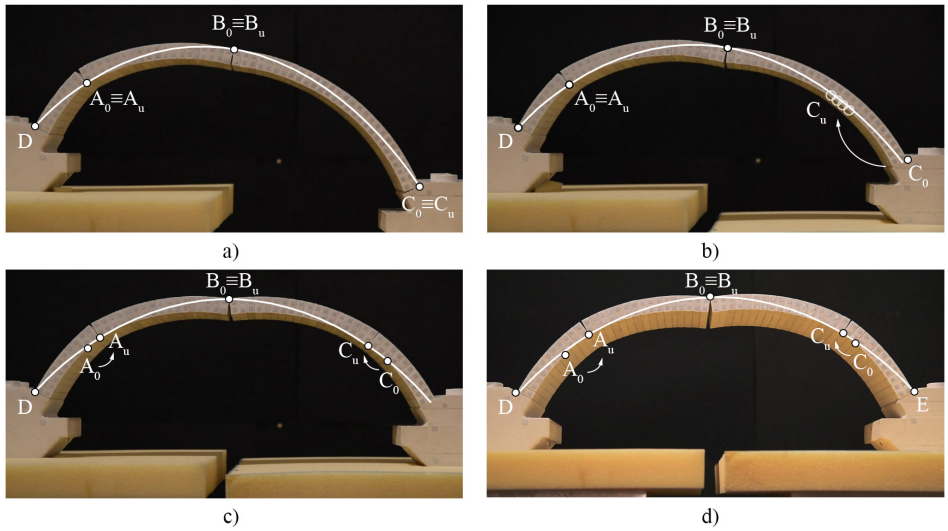

Fig. 2. Collapse mechanisms: a) α = 0°, b) α = 20°, c) α = 60°, d) α = 90° (the initial and final locations of hinges A, B and C are indicated as A_0, B_0, C_0 and A_u, B_u, C_u, respectively) (Ferrero, Calderini and Roca, 2022b).

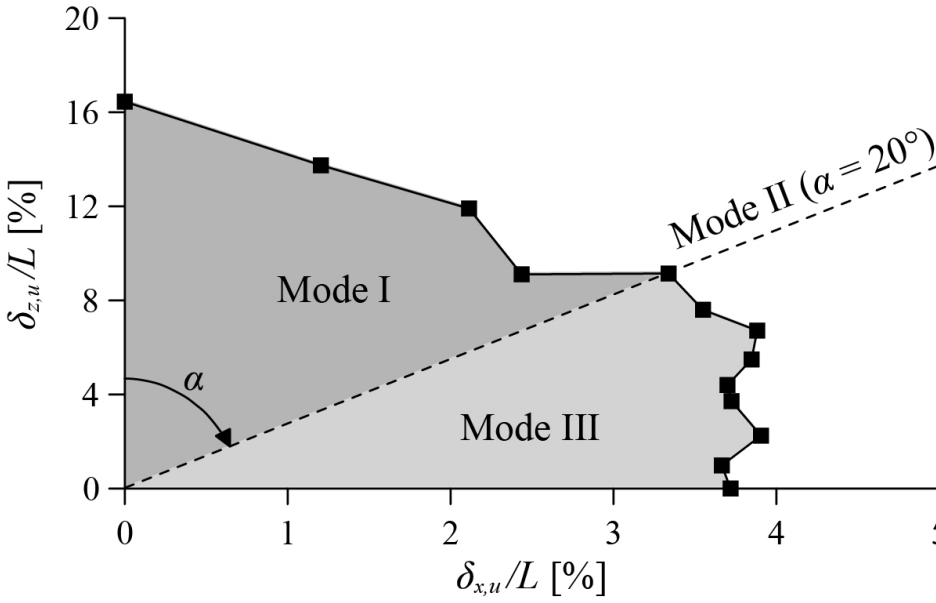

Fig. 3. Limit displacement domain of the tested arch (Ferrero, Calderini and Roca, 2022a).

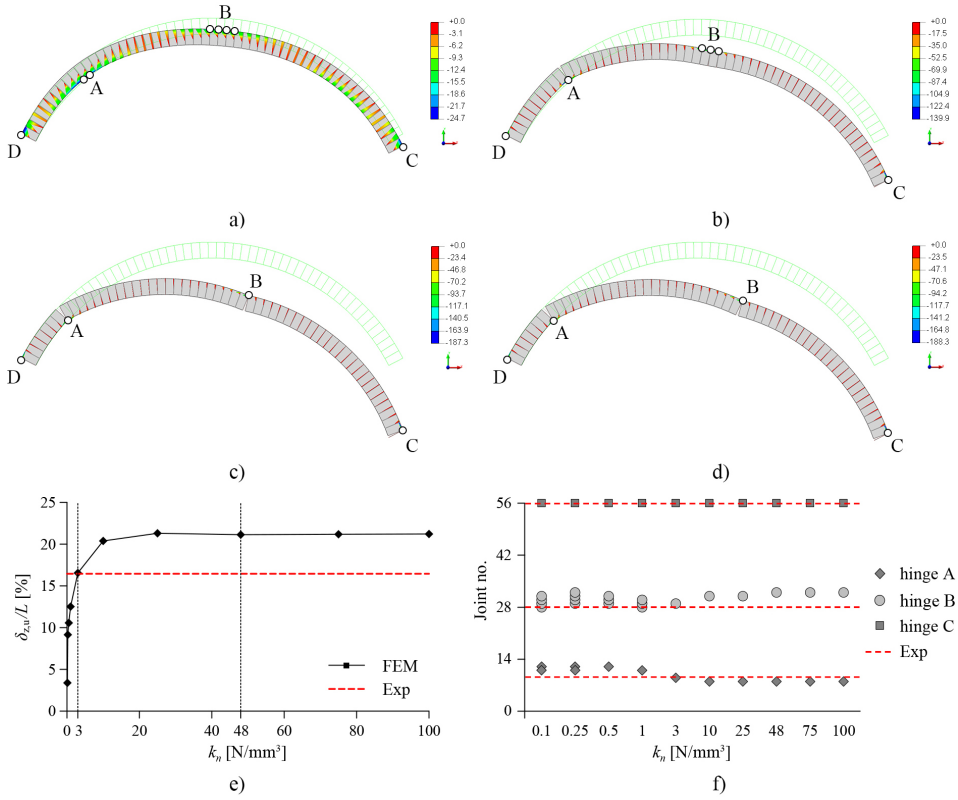

Fig. 4. Sensitivity analysis to the interface normal stiffness k_n: collapse mechanisms for (a) k_n = 0.1 N/mm³ ($\delta_{z,u}/L$ = 3.8%), (b) k_n = 1 N/mm³ ($\delta_{z,u}/L$ = 12.1%), (c) k_n = 10 N/mm³ ($\delta_{z,u}/L$ = 20.4%), (d) k_n = 100 N/mm³ ($\delta_{z,u}/L$ = 21.2%) (results in terms of compressive stresses in the interfaces); e) normalized collapse displacement $\delta_{z,u}/L$ vs. interface normal stiffness k_n; f) hinge position at collapse vs. interface normal stiffness k_n.. (Ferrero, Calderini and Roca, 2022b).

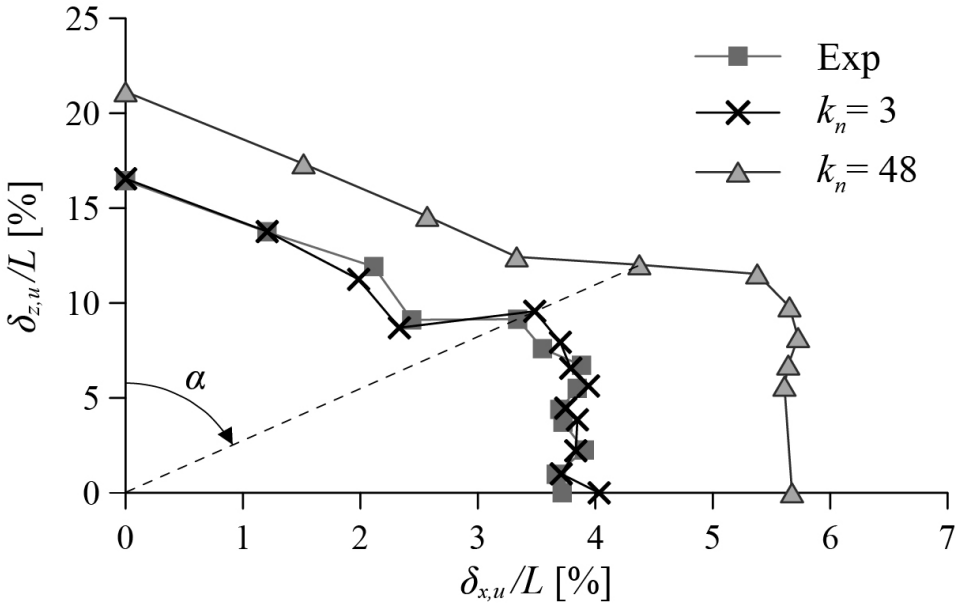

Fig. 5. Limit displacement domains of the tested arch obtained from experimental tests and FE analyses for both k_n = 3 N/mm^3 and k_n = 48 N/mm^3 (Ferrero, Calderini and Roca, 2022b).

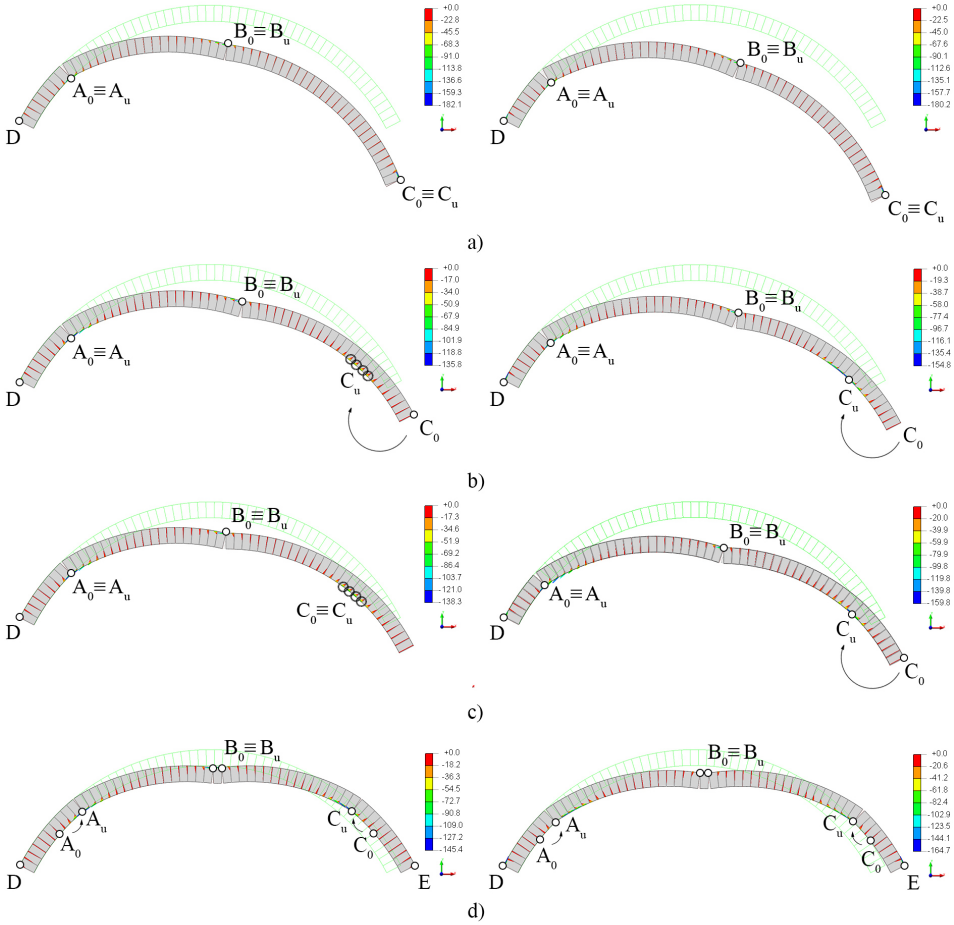

Fig. 6. Collapse mechanisms obtained from FE analyses for k_n = 3 N/mm³ (left) and k_n = 48 N/mm³ (right): a) α = 0°, b) α = 20°, c) α = 25°, d) α = 90° (Minor distributed openings are indicated with a dotted circle) (Ferrero, Calderini and Roca, 2022b).